Cassini Radio Detection and Ranging (RADAR): Earth and Venus observations

R. D. Lorenz

Lunar and Planetary Laboratory, University of Arizona, Tucson, Arizona

C. Elachi, R. D. West, W. T. K. Johnson, M. A. Janssen, M. Moghaddam, G. A. Hamilton, O. Liepack, A. Bunker, L. E. Roth, and S. D. Wall

Jet Propulsion Laboratory, California Institute of Technology, Pasadena, California

L. Dente, D. Casarano,[1] and F. Posa

Dipartimento Interateneo di Fisica, Istituto Nazionale per la Fisica della Materia, Bari, Italy

Abstract. The Cassini Radio Detection and Ranging (RADAR) was operated in scatterometric and radiometric modes during the Venus 1 and Earth swingbys to verify its functionality. At Venus, only the thermal emission from the thick absorbing atmosphere was detected. At Earth both the radar echo and the microwave emission from the surface were detected and reveal ocean surface disturbances, the rough, high, and cold Andes mountains, and surface features including a small reservoir in Brazil. Instrument performance appears to be excellent.

1. Introduction

The Cassini Radio Detection and Ranging (RADAR) instrument is a versatile Ku-band (13.8 GHz) instrument designed primarily to penetrate the thick haze-laden atmosphere of Saturn's satellite Titan. In addition, the instrument [*Elachi et al.*, 1991, 2001; *Borgarelli et al.*, 1998] will be used to observe Jupiter, Saturn, its rings, and its icy satellites.

The RADAR was developed jointly by Alenia Aerospazio of Italy and the Jet Propulsion Laboratory, Pasadena, California. The instrument uses the 4-m high-gain antenna on Cassini, with five feeds: One generates a 0.35° circular beam boresighted on the spacecraft $-Z$ axis; the other four provide four collinear elliptical beams. Each beam can be used independently, although the expected principal mode of operation is to use all four together with the center circular beam ("beam 3") to form a fan-shaped beam ~0.35° across and 5.75° wide for imaging.

The RADAR's prime mode of operation is as a synthetic aperture radar (SAR) mapper at Titan, with the fan-shaped beam dragged across Titan's surface during a close flyby to image a strip ("swath") of terrain some 150 km or so wide across track and several thousand kilometers long along track. These data will resemble somewhat (although at slightly lower spatial resolution) the images obtained by the Magellan spacecraft at Venus.

The RADAR has other operational modes, which, in general, use only beam 3, the central narrow beam (this was the only beam used at Venus and Earth). These modes are altimeter, scatterometer, and radiometer. The former two are sim-

ilar in that they record the echo power as a function of range: The bandwidth in the altimeter mode is wider to measure the range to the target more accurately (to build nadir-pointed topographic profiles with an altitude resolution of ~50 m), while in scatterometer mode a narrower bandwidth sacrifices range resolution for improved signal-to-noise ratio to measure the backscatter at a range of incidence angles.

During all of the active modes, SAR, altimeter, and scatterometer, the microwave power in the beam is also measured in intervals when no echo is expected: This allows the microwave emission of the surface (and thus either its emissivity or its temperature) to be measured. This radiometric mode can also be operated independently, with no active microwave transmission (and therefore using less spacecraft power). The target brightness temperatures are compared to on-board calibration sources and ideally with cold space.

During the Venus 1 and Earth encounters, the instrument was operated in scatterometer mode and additionally provided radiometer data. The RADAR was not expected to provide new information about either body but rather was operated to obtain calibration data and rehearse instrument operations.

2. Venus

The RADAR instrument was first operated in active (scatterometry) mode during Cassini's first flyby of Venus on April 26, 1998. Closest approach occurred at an altitude of 284 km, although RADAR operations were constrained to some time after closest approach, when Venus passed in front of the Sun-pointed field of view. (Throughout the inner solar system phase of the Cassini mission, the high-gain antenna (HGA) is required to point at the Sun to shade the optical instruments and the Huygens probe from insolation.)

No RADAR echo was detected. This was not unexpected, since severe pressure-induced absorption occurs at microwave frequencies in the thick Venusian atmosphere. This is apparent
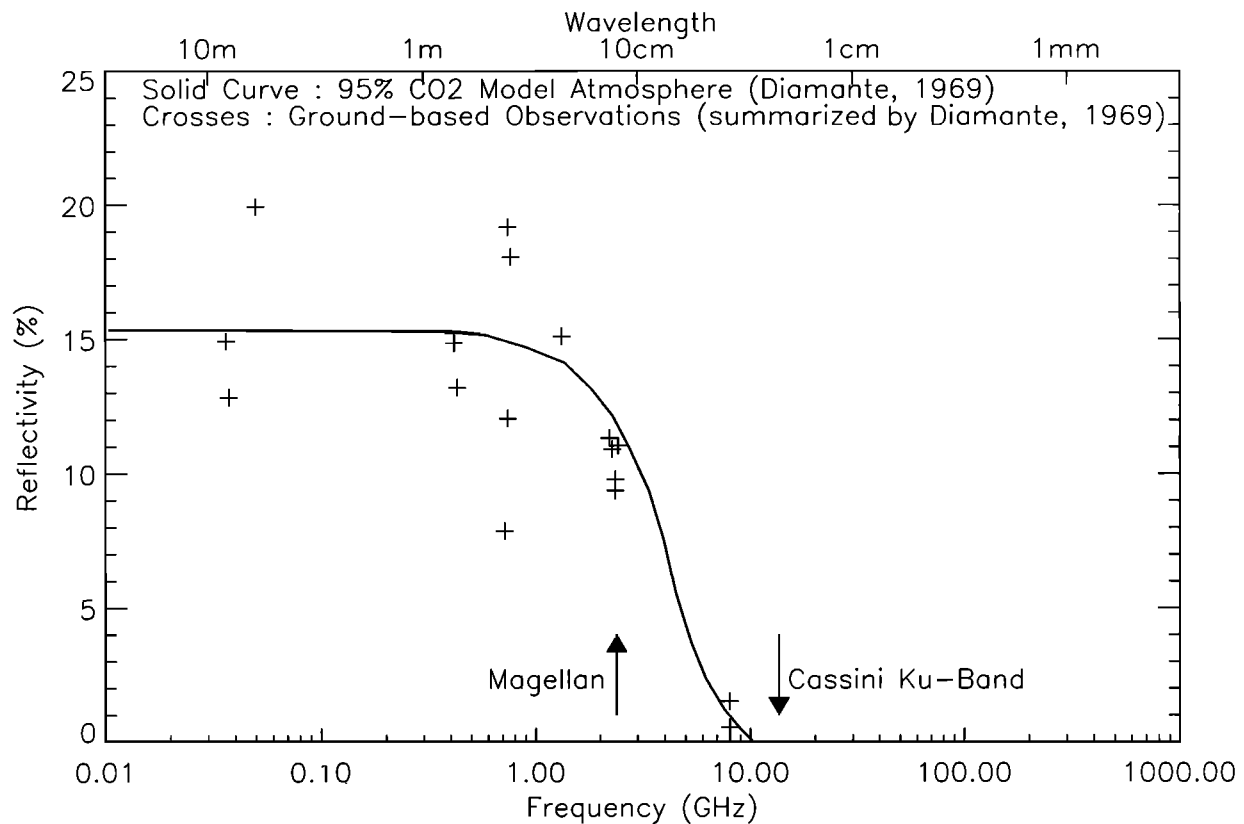

Figure 1. Radar reflectivity of the Venusian surface as a function of frequency. Absorption by the thick CO_2 atmosphere severely reduces the reflectivity above 2 GHz.

in early models and observations from Earth, summarized, for example, by *Diamante* [1969] (see Figure 1).

Of course, Venus's surface is visible to RADAR at longer wavelengths, where the atmospheric attenuation is less severe: Magellan spacecraft operated at S band (2.45 GHz), and Veneras 15 and 16 operated at 3.75 GHz. Venus's radar reflectivity shows a steep drop-off between 2 and 10 GHz: At Cassini's operating frequency of 13.8 GHz the expected return would be at best marginally detectable. Venus 1 operations were, however, intended principally as an engineering exercise.

In the raw radiometer data it was apparent that a warm object was present in the beam. However, because no cold sky reference measurement was taken before the Venus measurement, it was impossible to assign a meaningful brightness temperature. This brightness temperature would be somewhat lower than the surface thermodynamic temperature, again because of atmospheric attenuation; the unity optical depth level probed by the radiometer is at some (cooler) altitude above the surface (see Figure 2) [e.g., *Janssen*, 1993]. No RADAR operations were conducted during the Venus 2 flyby in June 1999.

3.   Earth

Cassini's Earth flyby provided an opportunity to test the RADAR instrument in active mode. Although the target object (the Earth's surface) is exceedingly complex in terms of its RADAR reflectivity, it is at least fairly well studied by other spaceborne radars. Furthermore, the flyby geometry is not unlike many of the close Titan flybys, such that the Earth

encounter provided valuable experience in sequencing an encounter.

Operational constraints on the Earth swingby provided significant challenges. First, the spacecraft attitude was restricted to maintain the $-Z$ axis (the HGA) toward the Sun to minimize thermal loads on the sensitive optical remote sensing (ORS) instruments and the Huygens probe. This lead to non-ideal (large, i.e., far from vertical) incidence angles near closest approach. Second, since RADAR is a ranging instrument, where the echo time should be well estimated a priori (to set the receive window), the ephemeris needs to be up-to-date and consistent with the instrument commands. For example, late maneuvers such as the debris avoidance maneuver which changed the time of closest approach, required change in instrument settings at short notice. Similar vigilance will be required at Titan.

Third, as is also expected during Titan encounters, RADAR has an overconstrained timeline, where many instruments with conflicting modes or pointing wished to operate. As a result, RADAR requested operation during only a short interval following closest approach.

Fourth, the absolute calibration of brightness temperatures is essentially impossible without a cold sky calibration, which (since the instrument was pointed at the Sun) was not available. Measurements at Jupiter and in the Saturnian system will not be handicapped this way. Cold sky measurements at Jupiter and during the Instrument Checkout-2 (ICO-2) presently ongoing in September 2000 will allow the construction of a better model of the noise sources and losses in the antenna
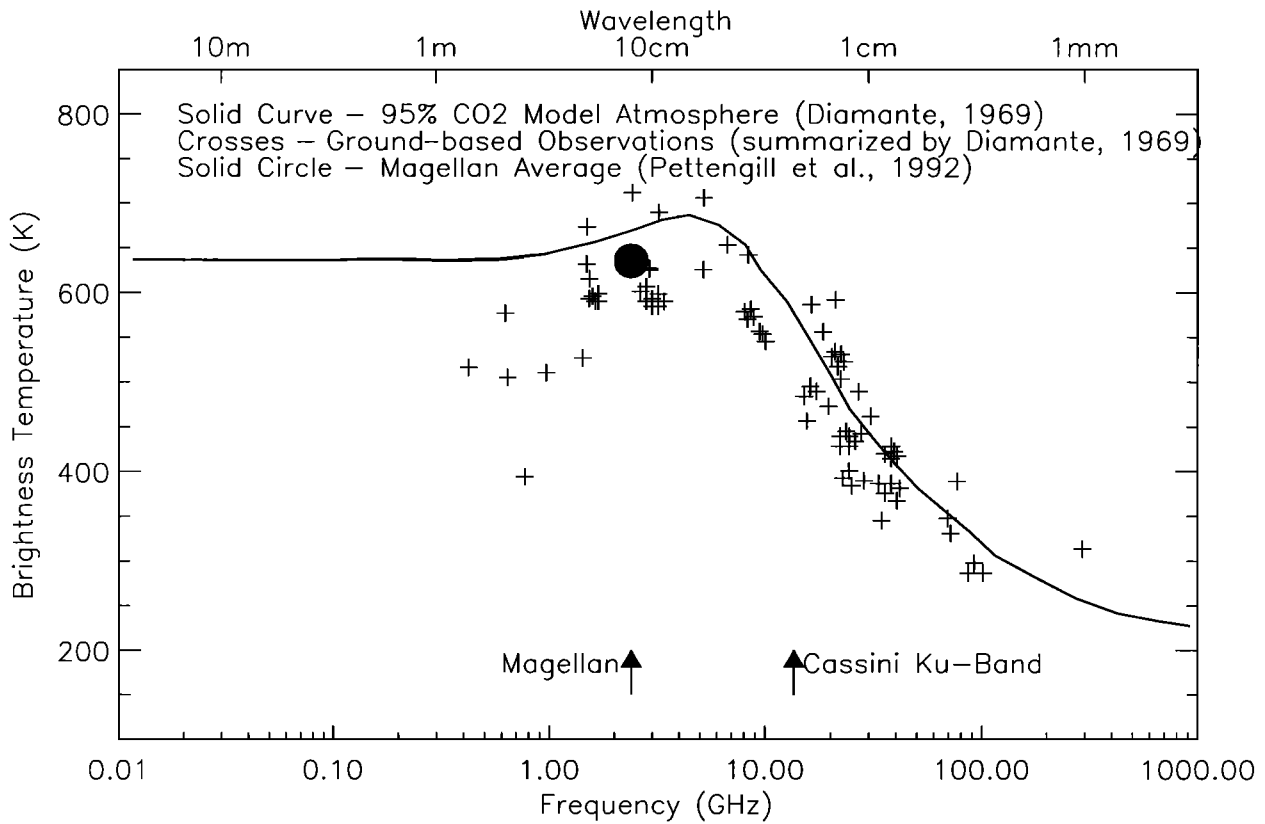
Figure 2. Brightness temperature of Venus as a function of frequency. Ku-band radiation does not quite probe the surface.

system, and may allow the retroactive estimation of the brightness temperature at Venus. Preliminary analyses of the Earth swingby observations were reported by West et al. [2000] and Casarano et al. [2000].

3.1. Observation Geometry

Of course, since the spacecraft was Sun-pointed throughout this period (Figure 3), it follows that the observation was made in darkness. When the radar instrument was activated about 550 s after closest approach (CA), the beam (pointing at the occulted Sun) intercepted the Earth's surface at 26.6°S, 87.1°W, in the eastern Pacific Ocean (see Figure 4). The incidence angle of 34° corresponds quite closely to that used in terrestrial scatterometer measurements of sea state and wind speed (typically 40°). At this moment, Cassini was ~6500 km from Earth.

The beam moved across the Earth's surface in an ENE direction, at landfall at CA + 770 s, 24.2°S, 71°W, just to the south of Antifagasta in northern Chile. At this range of 9100 km the beam (0.35° in diameter) footprint at an incidence angle of 19° was an ellipse 59 km × 56 km; throughout the rest of this paper we will consider a circular beam footprint as a sufficient approximation.

After the beam traversed the Andes, it skirted just south of the Bolivian border and crossed Paraguay. Over the Brazilian highlands the incidence angle reached a minimum of ~6.6° at 19.6°S, 53.3°W and then increased to 16°. These angles are close to those used for synthetic aperture radar (SAR) imaging.

A second land-ocean crossing would have been of consider-

able interest. However, to permit other investigations (Cassini Plasma Spectrometer (CAPS); see elsewhere in this issue) the RADAR observation was terminated at 1240 s after closest approach, with the beam footprint centered at 15.4°S, 39.9°W, only ~160 km from the coast.
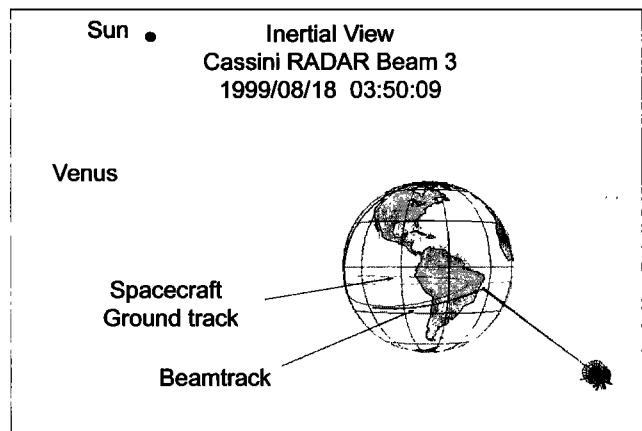

Figure 3. Viewing geometry at the Earth encounter. The Cassini spacecraft (not shown to scale) is moving toward the lower right as the Earth drifts right to left. The radar beam, pointed toward the Sun, first intersected the Earth's surface over the Pacific Ocean. The Cassini ground track has a U shape, with the apex close to the end of the RADAR observation; after that point, as the spacecraft's range increases, the Earth's rotation sweeps the subsatellite point westward.
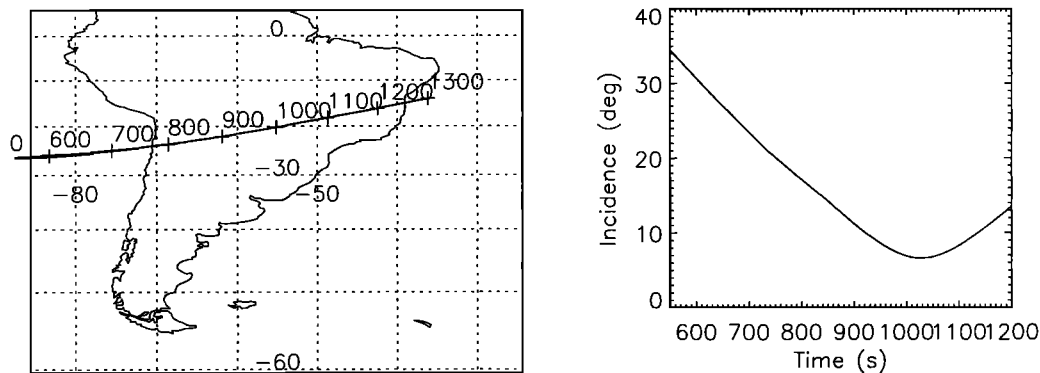
Figure 4. Ground track of the center of the beam during the Earth swingby and the evolution of incidence angle. The range varied smoothly from ~7000 to ~17,000 km during this interval.

The range from Cassini to the target at this point was some 16,500 km. This, incidentally, represents one of the most distant civilian radar observations of the Earth: most Earth observation spacecraft operate at altitudes of 1000 km or less.

3.2. Radiometer Data

The brightness temperature measured by the radiometer is typically dominated by the thermal emission (i.e., physical temperature and emissivity) of the surface at which the instrument is pointed. This will be the case for the icy satellites and Titan. For studying Saturn the absorption and scattering by water and

ammonia clouds will be significant. Microwaves at this frequency may also be generated by synchrotron emission around Jupiter; this will be the subject of a dedicated RADAR observation at Jupiter.

At Earth the expectations for Titan largely applied in that the surface conditions were the only significant determinant of the received signal. Although water vapor and precipitation in particular can affect Ku-band propagation in the atmosphere [e.g., *Ulaby et al.*, 1986], the conditions over South America according to the National Oceanic and Atmospheric Administration (NOAA) synoptic view at the time of the observation were essentially dry.
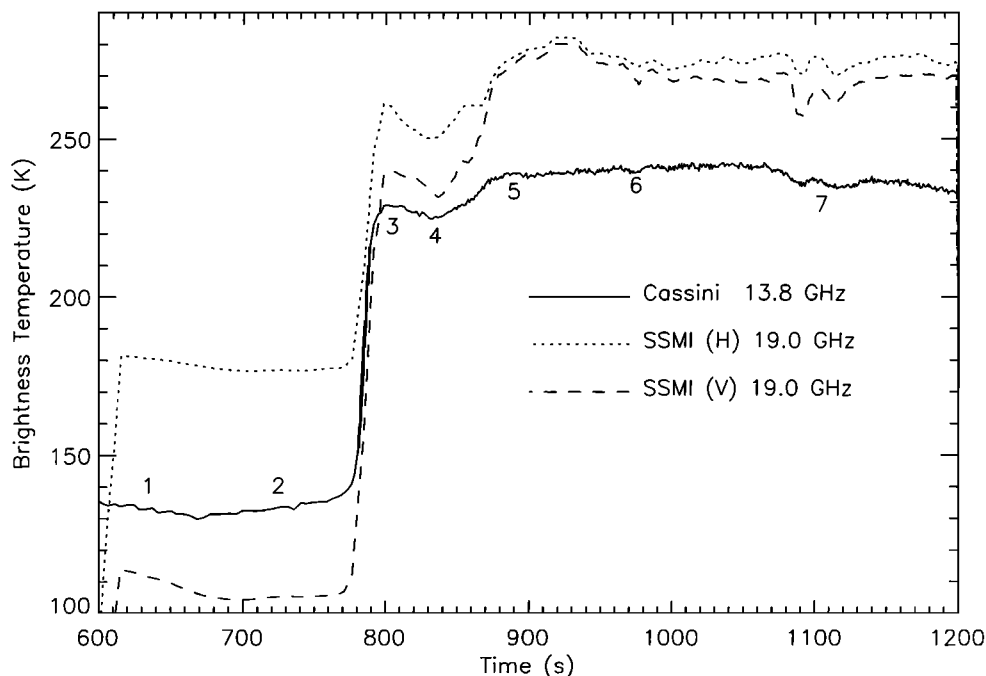

Figure 5. Uncalibrated brightness temperature recorded during the Earth encounter compared with typical brightness temperatures. Numbers mark features described in the text. Brightness is not particularly wavelength-dependent in dry conditions. Over the ocean, brightness is quite low, as expected, and (also as expected) the Cassini brightness lies between the Special Sensor Microwave Imager (SSMI) H and V (horizontally and vertically polarized) extremes. Over land the Cassini radiometer reads a little low (corrected in subsequent plots). The SSMI data are from a gridded product made from data obtained in the week around the Cassini encounter. In this and subsequent plots, the abscissa is referred to as "time" whereas, in fact, time is merely a convenient proxy for location.
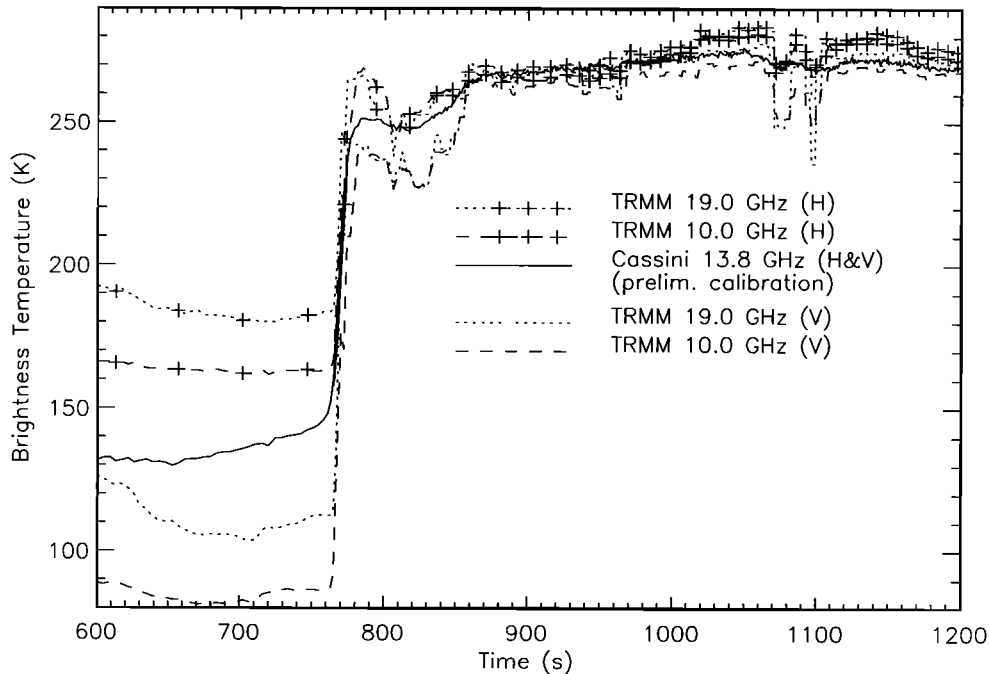
Figure 6. Cassini brightness temperature with preliminary calibration applied, showing good agreement with other data. Here near-simultaneous Tropical Rainfall Measurement Mission (TRMM) measurements at two wavelengths and two polarizations are shown; the Cassini data interpolate well between the 10- and 19-GHz frequencies. Small-scale features are muted in Cassini data, owing to beam dilution in Cassini's larger footprint. Toward the beginning of the observation the Cassini data are dominated by H-polarized emission, whereas toward the end, V polarization is the principal contributor. The data appear consistent with this change in bias, fitting the H curves better earlier and fitting the V curves better later.

Studying the radiometer data (Figure 5), we note several features.

1. Over the open ocean, sea surface temperature falls from west to east: This is a well-known ocean circulation feature as cool water moves north along the coast of South America.

2. Nearer the coast the brightness temperature begins to increase: This may be because of shallower littoral seas having less influence from the ocean current. There may also be a sea state effect (frothy seas are better emitters and hence have a higher brightness temperature).

Features 1 and 2 are not artifacts: They are also observed in the contemporaneous Tropical Rainfall Measurement Mission (TRMM) TRMM Microwave Imager (TMI) and Defense Meteorological Satellite Program (DMSP) Special Sensor Microwave Imager (SSMI) radiometer data at 10 and 19 GHz.

3. The brightness temperature over land is considerably higher. This local peak corresponds to the coastal plains.

4. Thermodynamic temperature falls with altitude: The minimum corresponds to the Andes Mountains in the Puna di Atacama, with an elevation of ~5 km.

5. Returning to lower terrain, now wooded grassland rather than shrubby or bare ground, the temperature rises.

6. This dip at 950 s appears to be a real feature, present in all data sets. The dips at 21.23°S, 58.5°W corresponds with marshland to the west of the River Nabilque in Paraguay. The elevation in this region is 0–200 m above sea level; the dip is not related (as over the Andes) to a rise in altitude.

7. This double dip corresponds with the Brazilian highlands. It was initially thought that altitude, perhaps in combination with different land cover (since this region is more

cultivated) was responsible. Landsat normalized difference vegetation index (NDVI) [*De Vries and Townshend*, 1994] shows a change in landcover from 6 (wooded grassland) to 11 (broadleaf deciduous forest and woodland) that is correlated with these dips. Further analysis (see section 3.3, Figure 10) indicates that in fact water is probably the principal influence here.

A model of the antenna system and receiver was constructed to take into account the losses and noise in the system. After tuning, the resultant brightness temperatures for Cassini data are more physically meaningful (although remember an absolute calibration is difficult without a cold sky background measurement). The results agree better with the "expected" brightness temperatures. To isolate possible temporal variations and explore the effect of wavelength and polarization variation, the Cassini data are plotted in Figure 6 against near-simultaneous observations by TRMM. The 13.8-GHz Cassini data interpolate well between TMI's 10- and 19-GHz observations. Small-scale features are muted in Cassini data owing to beam dilution in Cassini's larger footprint. Because of the viewing geometry dictated by Sun pointing, the polarization of the Cassini measurement varied throughout the encounter: Toward the beginning of the observation the Cassini data are dominated by H-polarized emission, whereas toward the end, V polarization is the principal contributor. The data appear consistent with this change in bias, fitting the TMI H curves better earlier and fitting the V curves better later. Although the results appear quite satisfactory, the radiometer model may nonetheless be improved after more cold sky and microwave source observations are taken during instrument checkouts in cruise.
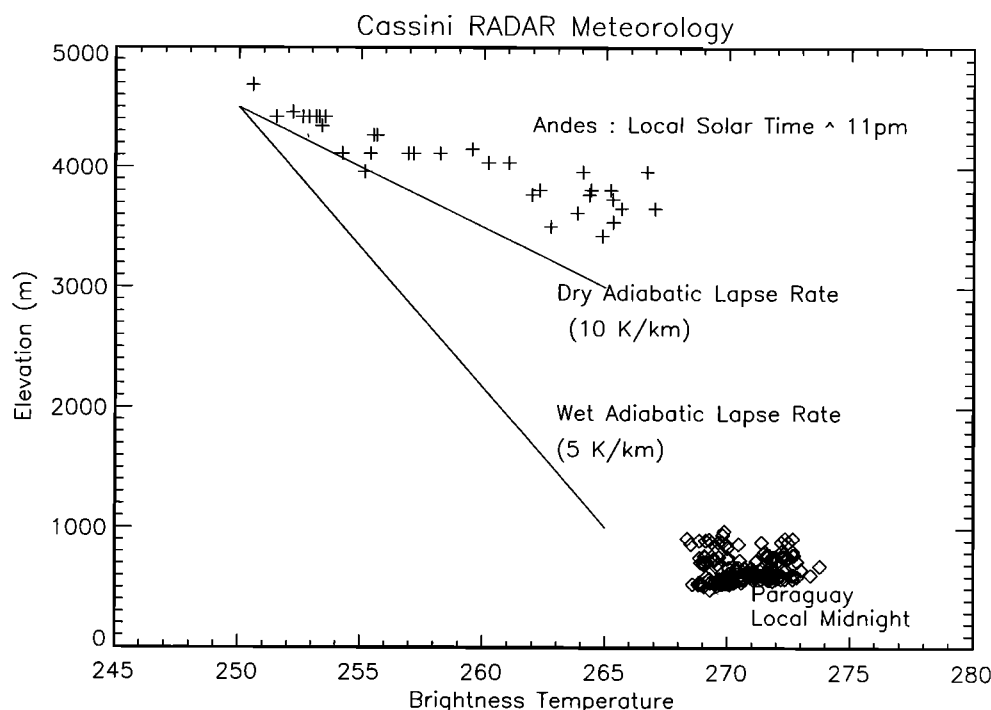
Figure 7. Elevation of the sensed region extracted from the ETOPO5 digital elevation model as a function of RADAR-sensed brightness temperature for selected data during the flyby. It is seen that the cold, high air of the Andes holds the surface temperatures to a dry adiabatic lapse rate, while to reach the warmer lowlands requires a steeper curve, consistent with convection in a somewhat moister atmosphere.

The meteorological potential of microwave radiometry is highlighted by the correspondence of the brightness temperature with altitude, shown in Figure 6. Altitudes were derived from the ETOPO5 digital elevation model [*NOAA*, 1988]. Over land the emission temperature corresponds fairly closely to but is slightly lower than the thermodynamic temperature (i.e., emissivity is slightly lower than unity). It can be seen that the temperatures for the high, dry Andes lie on a line with a slope of around 10 K km^{-1}, roughly equal to the dry adiabatic lapse rate. Extending the line fit to lower altitudes fails, underpredicting the temperatures. For the lowlands a steeper slope of around 5 K km^{-1} or more is needed (the change in local solar time also steepens the slope somewhat). A slope of 5 K km^{-1} corresponds quite closely to a wet adiabat, as might be expected at lower altitudes over South America, where the air is moister.

3.3. Backscatter Data

The radar backscatter profile (Figure 7) in many ways mirrors the brightness temperatures, with some important differences. Over the ocean at high incidence early in the observation, the backscatter is very low, consistent with a fairly smooth ocean surface. Backscatter from land was considerably (10 dB) higher. However, the transition from a low backscatter over ocean to a higher backscatter over land was somewhat puzzling, in that the transition in the backscatter curve appeared to occur some tens of seconds before it did so in the brightness temperature data.

In fact, this discrepancy highlights the superior sensitivity of active measurements to surface roughness, as highlighted with comparison to near-contemporaneous observations using the Quickscat scatterometer (see Figure 8). This is also a Ku-band

instrument, but with a fixed incidence angle of 49°. Data from day of year (DOY) 229, taken ~5 hours prior to the Cassini observation, have a very similar shape over the ocean, with a pronounced (20 dB) jump in backscatter at the location corresponding to ~650 s after CA. The absolute value of Cassini backscatter (with a preliminary calibration and noise subtraction applied) is rather higher than that for Quickscat because the Cassini incidence angle is rather lower (~26°) than Quickscat. A few hours after the Cassini observation, another Quickscat swath (DOY 230) shows that the ocean sea state has changed somewhat.

Backscatter is enhanced, although very variable, over the Andes and falls by several decibels (even though the incidence angle is becoming lower) to a minimum around t = 850 s. Again, the backscatter is higher than that recorded by Quickscat because of the lower incidence angle for Cassini. Studies of South America with scatterometers [e.g., *Kennett and Li*, 1989a; 1989b; *Birrer et al.*, 1982; *Hardin and Long*, 1994] show a typical variation of backscatter with incidence angle (a parameter often referred to as "*B*" or "beta") of 0.12 dB deg^{-1}. Applying this correction to the Cassini data brings it into quite good agreement with the Quickscat data until ~950 s. After this point (and indeed over the Andes Mountains) this correction fails to match the Quickscat data. The answer is almost certainly that while for the incidence angles most commonly used by scatterometers in these papers (25–50°) this 0.12 dB deg^{-1} value is appropriate, at lower incidence angles, and in particular over bare ground and cultivated lands, a larger B value (or rather, a nonlinear dependence of backscatter with incidence angle) is applicable [see, e.g., *Newbry*, 1960; *Ulaby et al.*, 1986; *Long*, 1998]. (In passing, it is worth noting that while the transect across ocean and the Andes is interesting, as an
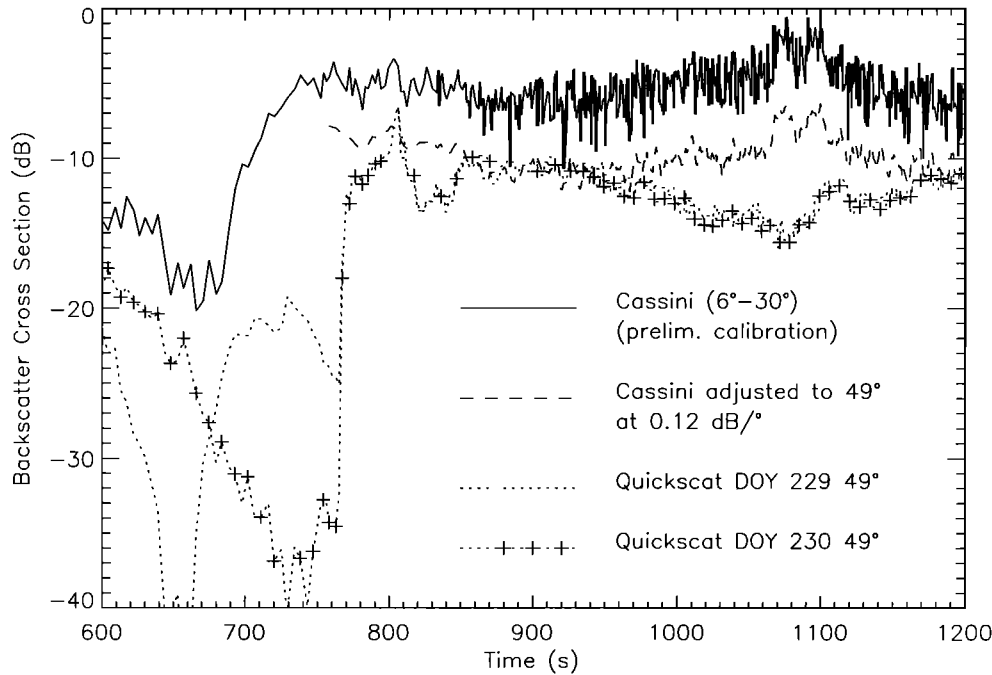
Figure 8. Comparison of Cassini backscatter with a preliminary calibration applied with Quickscat scatterometer. Data for day of year (DOY) 229 were taken ~4.5 hours prior to the Cassini observation; DOY 230 was taken ~5 hours afterward. The dramatic variation in backscatter across the ocean (600–770 s) is evident: The DOY 229 curve shows good correlation with the Cassini data. Variations are due, in part, to temporal changes and to incidence and azimuth differences. Over land the Cassini data show a much stronger backscatter than the 49° incidence Quickscat data, owing to the much lower incidence angle. Correction by 0.12 dB deg^{-1}, typical of wooded terrain, brings much better agreement, except between 950 and 1150 s, where bare ground and cultivated lands require a steeper incidence angle correction. The Cassini data look noisier after t = 850 s because smaller bins have been used to average the signal.

absolute calibration target, the Amazon rainforest some thousands of kilometers to the north would be preferable, since this area is extremely homogenous in its backscatter cross section. Reflections, largely from the forest canopy, show little variation with azimuth or season.)

As the incidence angle becomes even steeper, the deviation between Cassini and Quickscat becomes more pronounced, as expected from the discussion above. A remarkable and pronounced double peak is evident at around t = 1100 s, corresponding to the double dip in brightness temperature discussed before. The Quickscat data shed little light on this feature, but it can be seen from TRMM precipitation radar (PR) measurements (at equivalent incidence angles and frequencies to Cassini, 13.8 GHz; note also that no rain was present in the period around the observation) that this backscatter spike is real (Figure 9).

It was initially thought that this feature might be purely due to land cover. Agriculture and urbanization may be partly responsible but might be unlikely to account for the drop in brightness temperature. However, while at moderate incidence angles earlier, smooth water gives very weak backscatter since most radiation is specularly reflected away from the antenna, at the near-vertical incidence angles prevailing at t = 1100 s, smooth water gives very strong backscatter and would give a low brightness temperature as well. On close inspection it seems that water is indeed responsible. These spikes correspond to where the beam footprint crosses the reservoir created by the blockage of the Paranaiba River near Itmbaria by the San Simao dam (Figure 10). The footprint of the TRMM

PR is 5–10 times smaller than that of Cassini, so the sharp peaks in the TRMM data are diluted by Cassini's wider beam.

This discussion highlights the utility of simultaneous radiometer and backscatter measurements. Radiometrically, the Cassini data appear consistent with other measurements, and all features in the data appear to be understood in terms of surface features.

3.4. Ranging Data

In principle, the scatterometer mode is a low-resolution altimetric mode. Since there is a substantial topographical variation along the ground track (up to nearly 5 km), we attempted to detect this topography by looking for the time of the leading edge of the echo signal compared to where it would be expected for a spheroidal Earth. However, because of the high incidence angle, the poor signal-to-noise ratio prevented this approach from yielding a consistent profile. A template-fitting or centroid-finding approach may yet succeed in isolating a topographic signal: Such analyses are underway.

4. Conclusions and Prospects for Titan

The Earth swingby geometry was far from ideal for a radar observation: An ideal rehearsal of a Titan encounter would have allowed the spacecraft to turn to perform SAR imaging near closest approach.

However, the exercise has been very instructive, and the utility of combined radiometry and backscatter measurements has been evident. All the features in the data can be
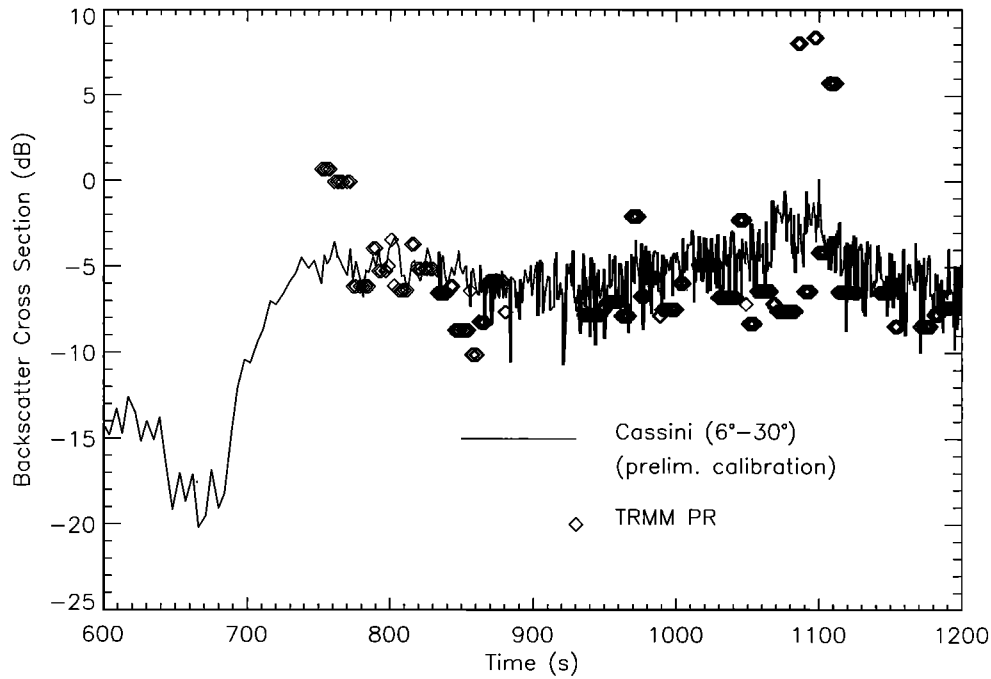
Figure 9. Cassini backscatter against TRMM precipitation radar (PR) sigma-0, recorded at equivalent (within 2° at each point) incidence angles over land. Note especially the sharp spikes around $t = 1100$ s: Again, these are muted in the Cassini data, which have a footprint of around 50-km diameter compared with that of the TRMM PR, which is near 4 km. The agreement, in general, is quite good: The large differences at $t = 770$ s and $t = 1120$ s are likely due to azimuth differences and the extreme variability of backscatter over short length scales in these regions.

related to real features on the ground. The simultaneous altimeter-radiometer record, simulated in Figure 7, will be a particularly interesting data set for understanding Titan's meteorology.

The noise performance of the radiometer has proven to meet or exceed expectations and promises excellent science at Saturn. (It may be noted in passing that in the original Cassini concept there was a separate radiometer instrument; ulti-
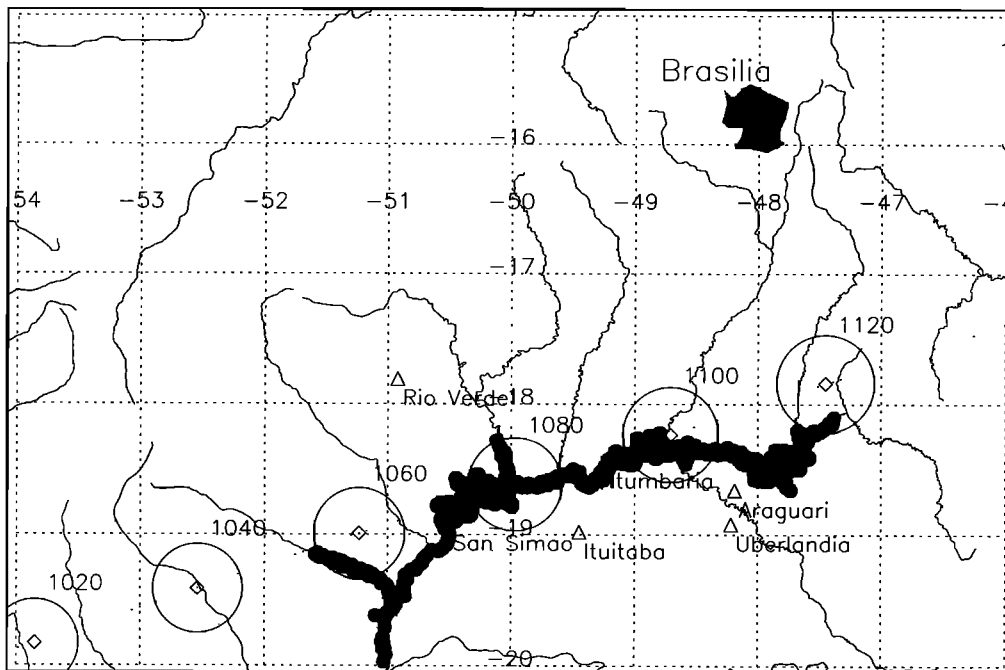

Figure 10. Beam footprints around the time of "anomalously high" returns around $t = 1100$ s. The peaks in backscatter correspond to where water (highlighted with solid circles) behind the San Simao dam fills the beam.

mately, that instrument was descoped into the radiometry mode of the RADAR.) The performance specification calls for ~2 K absolute brightness temperature measurement and 0.1 K relative.

This temperature measurement accuracy corresponds (with typical Titan lapse rates of 1.3 K km^{-1}) to elevation changes of ~70 m, more-or-less commensurate with the expected altimetry accuracy at Titan [Elachi et al., 2001]. Additionally, it is known from Voyager 1 infrared sounding that Titan's surface temperatures fall off with latitude, with an equator-to-pole contrast of several degrees [Samuelson et al., 1997]. This contrast is higher than might be expected from zonal energy balance models that scale meridional heat transfer with pressure, although it is consistent with a principle of maximum entropy production [Lorenz et al., 2001]: It may be that condensation processes play a significant role [Stevenson and Potter, 1986].

Although the backscatter data look fairly noisy, it must be remembered that Cassini will take backscatter data at Titan under much more favorable circumstances, with the instrument footprint being allowed to dwell on the surface to allow more pulses to be integrated and thus the signal-to-noise ratio to be improved. Although SAR was not performed at Earth, most of the relevant subsystems have been exercised.

Although it taught us little we did not already know about the Earth's land and sea, the Earth swingby experience shows that even in its one-dimensional modes, RADAR can obtain interesting data on a planetary surface. The instrument performance bodes well for the Saturnian system and the application of its richest operational mode, SAR imaging, to Titan's land and sea.

References

Birrer, I. J., E. M. Bracalente, G. J. Dome, J. Sweet, and G. Berthold, Sigma-0 signature of the Amazon rain forest obtained from the Seasat scatterometer, *IEEE Trans. Geosci. Remote Sens., GE-20*, 11–17, 1982.

Borgarelli, L., E. Im, W. T. K. Johnson, and L. Scialanga, The microwave sensing in the Cassini mission: The Radar, *Planet. Space Sci., 46*, 1245–1256, 1998.

Casarano, D., L. Dente, F. Posa, R. L. Kirk, R. D. Lorenz, S. D. Wall, and R. D. West, Cassini Radar: Data analysis of the Earth flyby and simulation of Titan flyby's data, paper presented at Symposium on Remote Sensing, EUROPTO, Barcelona, Spain, Sept. 2000.

De Vries, R. S., and J. R. G. Townshend, NDVI-derived landcover classification at a global scale, *Int. J. Remote Sens., 15*, 3567–3586, 1994.

Diamante, J. M., The structure and circulation of the lower atmosphere of Venus, Ph.D. dissertation, Inst. for Space Stud., Goddard Space Flight Cent., Greenbelt, Md., 1969.

Elachi, C., E. Im, L. E. Roth, and C. L. Werner, Cassini Titan radar mapper, *Proc. IEEE, 79*, 867–880, 1991.

Elachi, C., et al., RADAR: The Cassini Titan radar mapper, *Space Sci. Rev.*, in press, 2001.

Hardin, P. J., and D. G. Long, Discriminating between tropical vegetation formations using reconstructed high-resolution Seasat-A scatterometer data, *Photogramm. Eng. Remote Sens., 60*, 1453–1462, 1994.

Janssen, M. A., *Atmospheric Remote Sensing by Microwave Radiometry*, John Wiley, New York, 1993.

Kennett, R. G., and F. K. Li, Seasat over-land scatterometer data, part 1, Global overview of the ku-band backscatter coefficients, *IEEE Trans. Geosci. Remote Sens., 27*, 592–605, 1989a.

Kennett, R. G., and F. K. Li, Seasat over-land scatterometer data, part 2, Selection of extended area land-target sites for the calibration of spaceborne scatterometers, *IEEE Trans. Geosci. Remote Sens., 27*, 779–788, 1989b.

Long, D. G., Comparison of TRMM and NSCAT observations of surface backscatter over the Amazon rain forest, paper presented at 8th International Geoscience and Remote Sensing Symposium, Inst. of Electr. and Electron. Eng., Edinburgh, 1998.

Lorenz, R. D., J. I. Lunine, P. G. Withers, and C. P. McKay, Titan, Mars and Earth: Entropy production by latitudinal heat transport, *Geophys. Res. Lett., 28*, 415–418, 2001.

Newbry, L. E., Terrain radar reflectance study, *Photogramm. Eng. Remote Sens., 26*, 630–637, 1960.

National Oceanic and Atmospheric Administration (NOAA), Digital Relief of the Surface of the Earth, www.ngdc.noaa.gov/mgg/global/etopo5.HTML, Natl. Geophys. Data Cent., Boulder, Colo., 1988.

Pettengill, G. H., P. G. Ford, and R. J. Wilt, Venus surface radiothermal emission as observed by Magellan, *J. Geophys. Res., 97*, 13,091–13,102, 1992.

Samuelson, R. E., N. R. Nath, and A. Borysow, Gaseous abundances and methane supersaturation in Titan's troposphere, *Planet. Space Sci., 45*, 959–980, 1997.

Stevenson, D. J., and A. E. Potter, Titan's latitudinal temperature distribution and seasonal cycle, *Geophys. Res. Lett., 13*, 93–96, 1986.

Ulaby, F. T., R. K. Moore, and A. K. Fung, *Microwave Remote Sensing: Active and Passive*, vol. 3, *From Theory to Applications*, Artech House, Norwood, Mass., 1986.

West, R. D., M. Moghaddam, W. T. K. Johnson, M. A. Janssen, G. A. Hamilton, O. Liepack, A. Bunker, A. C. Berkun, and L. E. Roth, Cassini observes the Earth with ku-band radar and radiometry, paper presented at 10th International Geoscience and Remote Sensing Symposium, Inst. of Electr. and Electron. Eng., Honolulu, Hawaii, 2000.

A. Bunker, C. Elachi, G. A. Hamilton, M. A. Janssen, W. T. K. Johnson, O. Liepack, M. Moghaddam, L. E. Roth, S. D. Wall, and R. D. West, Jet Propulsion Laboratory, California Institute of Technology, 4800 Oak Grove Drive, Pasadena, CA 91109.

D. Casarano, ENEA CR Trisaia, 75026 Rotondella, Italy.

L. Dente and F. Posa, Dipartimento Interateneo di Fisica, INFM, I-70126 Bari, Italy.

R. D. Lorenz, Lunar and Planetary Laboratory, University of Arizona, Tucson, AZ 85721-0092.